

YolOOD: Utilizing Object Detection Concepts for Out-of-Distribution Detection

Alon Zolfi¹, Guy Amit¹, Amit Baras¹, Satoru Koda², Ikuya Morikawa², Yuval Elovici¹, Asaf Shabtai¹

¹Ben-Gurion University of the Negev, Israel

{zolfi, guy5, barasa}@post.bgu.ac.il, {elovici, shabtaia}@bgu.ac.il

²Fujitsu Limited, Japan

{koda.satoru, morikawa.ikuya}@fujitsu.com

Abstract

Out-of-distribution (OOD) detection has attracted a large amount of attention from the machine learning research community in recent years due to its importance in deployed systems. Most of the previous studies focused on the detection of OOD samples in the multi-class classification task. However, OOD detection in the multi-label classification task remains an underexplored domain. In this research, we propose YolOOD – a method that utilizes concepts from the object detection domain to perform OOD detection in the multi-label classification task. Object detection models have an inherent ability to distinguish between objects of interest (in-distribution) and irrelevant objects (e.g., OOD objects) on images that contain multiple objects from different categories. These abilities allow us to convert a regular object detection model into an image classifier with inherent OOD detection capabilities with just minor changes. We compare our approach to state-of-the-art OOD detection methods and demonstrate YolOOD’s ability to outperform these methods on a comprehensive suite of in-distribution and OOD benchmark datasets.

1. Introduction

Machine learning and particularly deep learning-based networks have become a state-of-the-art solution for computer vision tasks, such as image classification [9, 16], object detection [30, 31], and image segmentation [3, 4]. However, it has been shown that these models can produce overconfident predictions on samples out of the distribution they were trained on, *i.e.*, OOD samples [26].

Over the last few years, many solutions have been proposed to address this problem, most of which focus on the separation of in-distribution and OOD data [1, 13, 17, 18, 24, 36]. However, these studies only proposed solutions for the multi-class classification task, in which an input is associated with a single class category. The problem of OOD detection in the multi-label classification domain has been un-

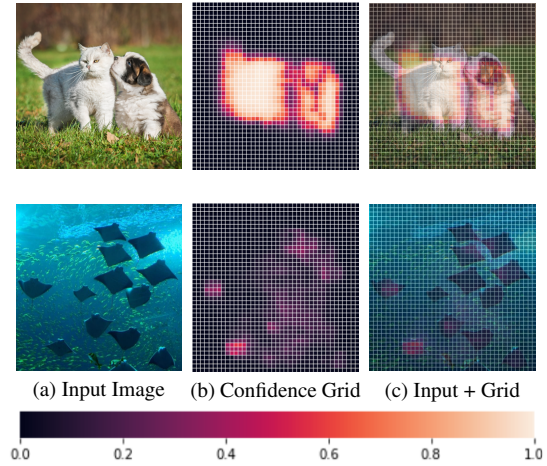


Figure 1. In-distribution image (top) and OOD image (bottom) with corresponding YolOOD confidence heatmap for each image.

derexplored, with just a single study performed by Wang *et al.* [39] that specifically addressed this domain.

Object detection is an extension of the multi-label problem, where in addition to predicting the multiple classes of the objects in an image, the model should also predict the exact location of the objects in the image. Object detectors have the inherent ability to distinguish between objects of interest and irrelevant objects [22, 30, 31]. This ability, along with object detection similarity to multi-label classification, can be leveraged to create an OOD detection mechanism for the multi-label setting.

In this paper, we propose *YolOOD*, a multi-label classifier that utilizes the main concepts of state-of-the-art object detectors, and specifically, the YOLO object detector [2, 14, 30]. To convert YOLO’s network into an image classifier, we simply replace the last layer of each detection head. *YolOOD* is based on the objectness score concept, which is commonly used in object detectors [28, 31] to understand the relevance of the different parts of the image.

This concept is realized by training the network to predict low scores for background areas in the image or areas that contain irrelevant objects. In terms of OOD detection, this can be interpreted as assigning low scores to OOD data.

As opposed to existing OOD methods in which the networks are actively trained on negative data from an external OOD data source [12, 25], *YoLOOD* offers a major advantage as it exploits all parts of the image to model both the original data distribution and objects that might be OOD, without the need for external data sources.

To demonstrate the effectiveness of *YoLOOD*, we perform extensive evaluations which demonstrate *YoLOOD*'s state-of-the-art performance and ability to outperform commonly used OOD detection methods on a large-scale benchmark image dataset (MS-COCO [20]). We also provide two OOD benchmark datasets that better capture the complexity of the multi-label setting in which images may contain multiple objects belonging to different class categories. The new datasets are: (a) a subset of the Objects365 dataset [34], and (b) a subset of the TACO dataset [27]. Our results show that *YoLOOD* substantially improves the FPR95 compared to the other OOD detection methods examined (*e.g.*, when using MS-COCO as the in-distribution dataset and the subset from Objects365 as the OOD dataset, the FPR95 decreases by 10.88%).

We summarize our contributions as follows:

- We propose *YoLOOD*, a novel OOD detection technique powered by the YOLO object detection system for the multi-label image classification domain that outperforms state-of-the-art techniques.
- We present a unique technique that exploits all parts of an input image to model both the original data distribution and what may be OOD, without depending on external data sources.
- We introduce two new OOD datasets that better reflect the complexity of OOD detection in the multi-label domain (*i.e.*, images may contain multiple objects of different class categories), and make them available to the scientific community.

2. Related Work

2.1. Object Detection

Object detectors have been studied extensively over the last few years demonstrating state-of-the-art performance, and various solutions aimed at identifying the objects present in an image and their precise location (*i.e.*, bounding box) have been proposed. Modern deep learning-based object detectors are usually composed of two components, a backbone network (usually pretrained on ImageNet [32]) and a head which is used to predict the bounding boxes and classes of existing objects in an image. These

models can be roughly categorized into two types: one-stage detectors (*e.g.*, SSD [22] and YOLO [2, 14, 30]) and two-stage detectors (*e.g.*, Mask R-CNN [8] and Faster R-CNN [31]). Object detectors developed in recent years often insert additional layers between the backbone and the head, which are used to collect feature maps from different stages. Models employing this technique include the Feature Pyramid Network [19], Path Aggregation Network (PAN) [21], BiFPN [37], and NAS-FPN [7]. In this paper, we focus on the YOLO one-stage object detector.

2.2. Out-of-Distribution Detection

Deep neural networks' overconfidence for OOD data was first noted by Nguyen *et al.* [26]. Several baseline approaches have been proposed to tackle this problem; for example, Hendrycks *et al.* proposed two baselines: the maximum softmax probability (MSP) [11] and MaxLogit, which uses the highest score from the classifier's last layer as an OOD score [10] (considered a baseline for OOD detection in the multi-label setting).

In recent years, OOD detection has attracted the attention of the machine learning research community, and researchers have proposed methods aimed at improving OOD uncertainty estimation, such as: (1) ODIN [18], which combines input preprocessing and temperature scaling; (2) the Mahalanobis [17] distance-based approach, which utilizes the network's internal feature representations; (3) the gradient-based GradNorm [13] score; (4) ReAct [36], which rectifies activation values; (5) IsoMax [24], which proposes isotropy maximization loss; and (6) the energy score [23]. These studies only addressed the multi-class classification task, and the topic of OOD detection in the multi-label domain remains largely underexplored. That domain has only been addressed by Wang *et al.* [39], who proposed JointEnergy which combines label-wise energies over all labels for OOD detection in the multi-label setting.

It should be noted that the OOD detection methods proposed in many prior studies require *external* OOD data (in addition to the OOD test dataset) to improve the detector's robustness. In some cases, the model is provided with OOD samples for hyperparameter tuning [18], while in other cases, these samples are used for negative learning in which the model is explicitly trained on images that do not contain in-distribution data [12, 25]. In contrast, object detection models in general, and YOLO in particular, do not require any type of external OOD data to model irrelevant objects and background areas.

3. Background

3.1. Multi-Label Classification

The multi-label classification problem is defined as follows: let \mathcal{X} be the input space and \mathcal{Y} be output space of

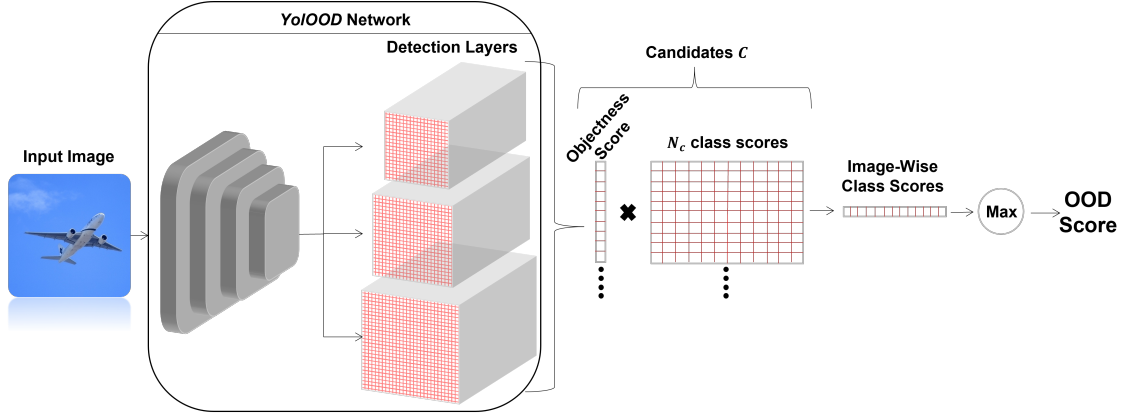


Figure 2. An overview of YoLOOD’s pipeline.

classifier $f : \mathcal{X} \rightarrow \mathbb{R}^{|\mathcal{Y}|}$ trained on samples drawn from distribution $\mathcal{D}(\mathcal{X}, \mathcal{Y})$. Every input $x \in \mathcal{X}$ can be associated with a subset of labels $\mathcal{Y} = \{1, 2, \dots, N_c\}$, which is represented by a binary indicator vector $y = \{0, 1\}^{N_c}$, where $y_n = 1$ if the input is associated with class n . Object detection is a variant of the multi-label classification task, in which the model also determines the location of existing objects, *i.e.*, bounding box coordinates.

3.2. YOLO Object Detector

In this paper, we focus on the state-of-the-art one-stage YOLO object detector and utilize its capabilities. Since the emergence of YOLO’s first version [28], other versions have been proposed to further enhance its performance [2, 14, 29, 30]. However, since YOLOv3 [30], the architectural design of the network has not been substantially altered; this design serves as the foundation for the recent state-of-the-art versions (*e.g.*, YOLOv4 [2], YOLOv5 [14]) and is utilized in our proposed approach.

YOLO’s architecture. YOLO’s architecture is comprised of two components: (a) a backbone network used to extract features from the input image, and (b) three detection heads which process the image’s features at three different scales. These components are connected using the feature pyramid network (FPN) [19] topology, where feature maps from different blocks of the backbone are concatenated to feature maps of corresponding sizes in the detection heads. The detection heads’ sizes are determined by the size of the input image and the network’s *stride* (downsampling factor) – 32, 16, and 8. This allows the network to detect objects of different sizes: the first detection head (with the largest stride) has a broader context, specializing in the detection of large objects, while the smallest one has better resolution and specializes in the detection of small objects.

YOLO’s detection layer. The last layer of each detection head predicts a 3D tensor of size $M \times M \times (4 + 1 + N_c)$,

where $M \times M$ is the grid size and $(4 + 1 + N_c)$ (which will be referred to as a *candidate* in the remainder of the paper) encodes three parts:

- Bounding box offsets - four coordinate offsets from a predefined anchor box.
- Objectness score - a single value that represents the model’s confidence that the bounding box contains an object.
- Class scores - N_c confidence scores indicating the presence of specific class categories.

To be more precise, every cell in the grid predicts three bounding boxes (associated with three predefined anchor boxes), resulting in a $3 \times M \times M \times (4 + 1 + N_c)$ prediction.

Training YOLO. Every ground-truth object is associated with a specific cell in each detection head. The input image is divided into an $M \times M$ grid, and the responsible cell is determined by the grid cell that the object’s center falls in. Since each cell contains three candidates, each of which is associated with a different predefined anchor box, the specific candidate is chosen to be the one with the highest intersection over union (IoU) between the ground-truth bounding box and the candidate’s anchor box.

YOLO does not assume that the class categories are mutually exclusive; therefore the class score vector is trained under the multi-label configuration (the sigmoid function is applied to each output neuron).

Postprocessing. YOLO outputs a fixed amount of candidates (depends on the input image size) which are then filtered in three sequential steps:

- Objectness score filtering - only candidates whose objectness score surpasses a predefined threshold are passed to the next step.

- Class score filtering - only candidates that have at least one unconditional class score ($Pr(Objectness) \cdot Pr(Class)$) that surpasses the predefined threshold are passed to the next step.
- Non-maximum suppression (NMS) - since many candidates can detect the same object, NMS is applied to reduce redundancy.

3.3. Out-of-Distribution Detection

Let \mathcal{D}_{in} denote the marginal distribution of \mathcal{D} over X , which represents the distribution of in-distribution data. At inference time, the system may encounter an input drawn from a different distribution \mathcal{D}_{out} over \mathcal{X} . For OOD detection in the multi-label setting, a decision function G is defined such that:

$$G(x; f) = \begin{cases} 1 & \text{if } x \sim \mathcal{D}_{in} \\ 0 & \text{if } x \sim \mathcal{D}_{out} \end{cases} \quad (1)$$

where x is considered OOD if none of the objects present in it are in-distribution objects.

4. Method

In this section, we introduce *YolOOD*, a novel OOD detection method for the multi-label domain, inspired by the YOLO object detector [14].

Object detectors have an inherent ability to distinguish between objects of interest (in-distribution data) and irrelevant objects (OOD data), making them perfect candidates for fulfilling the goals of the OOD detection task. Therefore, object detectors provide a natural solution for OOD detection. Another advantage of object detectors with regard to OOD detection pertains to their training procedure. The training of object detectors includes *passive negative learning* in which the unlabeled data present in the training images (*i.e.*, areas that are not included within labeled bounding boxes) enables the model to better generalize to the sub-task of discarding irrelevant objects; in YOLO, this is accomplished using the objectness scores.

With just minor changes, we convert the YOLO network into a multi-label image classifier, as explained in detail throughout this section.

4.1. YolOOD Detection Layer

Since we propose a method for the image classification domain, our model does not have to predict bounding boxes coordinates. Therefore, we replace the last layer of each detection head with a 3D tensor of size $M \times M \times (1 + N_c)$, so that the $M \times M$ grid remains identical to the grid in the original YOLO architecture, where each cell only predicts the objectness score and N_c class scores (as opposed to a candidate in the original YOLO that also predicts bounding box coordinates).

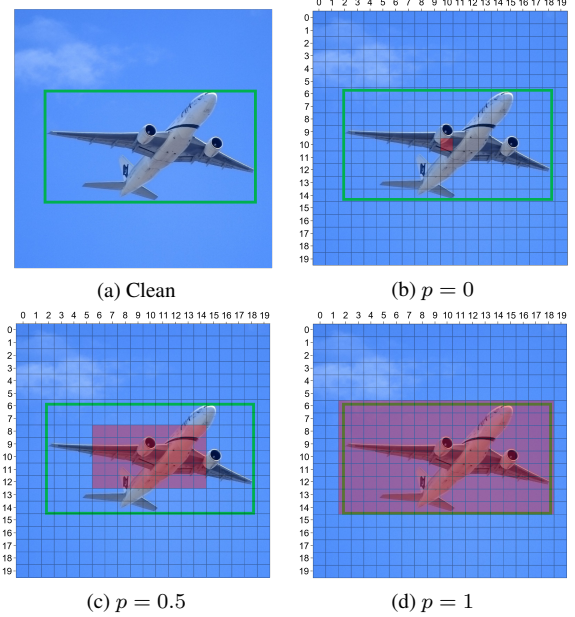


Figure 3. An example of an image divided into a grid of size 20×20 with various p values. The ground-truth bounding box is framed in green. Grid cells in red represent the responsible cells (as explained in Section 4.2).

Formally, let $f_{YolOOD} : \mathcal{X} \rightarrow \mathcal{C}$ be a *YolOOD* image classifier that receives an input image $x \in \mathcal{X}$ and outputs a set of candidates $f_{YolOOD}(x) = \mathcal{C}$ such that $\mathcal{C} = \bigcup_k \mathcal{C}_k$, where \mathcal{C}_k denotes the candidates of the k^{th} detection head ($k \in \{1, 2, 3\}$). Each set of candidates \mathcal{C}_k is comprised of $M_k \times M_k$ candidates (based on the downsampling factor mentioned in Section 3), and thus $|\mathcal{C}| = \sum_{k=1}^3 |\mathcal{C}_k| = (M_1^2 + M_2^2 + M_3^2)$.

4.2. YolOOD Objectness Score

As explained in Section 3, in the original YOLO model, only a single cell grid is responsible for the detection of an object. However, in the image classification task, we are not limited to the case of a specific cell predicting the object’s bounding box. Therefore, we propose enlarging the “responsibility” areas, such that multiple grid cells which contain *any* part of an object are responsible for detecting it, allowing the model to capture broader representations of objects.

However, an important aspect to consider is that bounding boxes do not accurately segment the object, *i.e.*, objects’ shapes are not necessarily rectangular, and the bounding box may include background areas that are not part of the object. This might result in incorrect associations of irrelevant parts inside the object’s bounding box with the object. Therefore, we propose using only a portion of the grid cells that cover the object’s area.

More formally, let (W_g, H_g) be the width and height of the grid and (W_o, H_o) be the normalized width and height of an object. The relative width and height of an object in a specific grid is defined as: $(W', H') = (W_o \cdot W_g, H_o \cdot H_g)$. In addition, let $(x_{\text{center}}, y_{\text{center}})$ denote the indices of the cell that the object's center falls in within a specific grid. We define p as the portion of grid cells relative to the grid's size, with regard to the object's center, *i.e.*, the responsible grid cells are expanded from the object's center to the object's boundaries as a function of p , as shown in Figure 3. When $p = 0$, the responsible cells are identical to those of the original YOLO model, while when $p = 1$, the responsible cells cover the area of the entire object. A candidate $c \in \mathcal{C}_k$ at location (i, j) in the grid is considered responsible for the detection of an object if the following conditions are satisfied:

$$\begin{aligned} \varphi_u = i \geq x_{\text{center}} - p \cdot \frac{W'}{2}, \varphi_l = j \geq y_{\text{center}} - p \cdot \frac{H'}{2} \\ \varphi_d = i \leq x_{\text{center}} + p \cdot \frac{W'}{2}, \varphi_r = j \leq y_{\text{center}} + p \cdot \frac{H'}{2} \end{aligned} \quad (2)$$

$$c_{\text{obj}}(i, j) = \begin{cases} 1 & \varphi_u \wedge \varphi_d \wedge \varphi_l \wedge \varphi_r \\ 0 & \text{else} \end{cases} \quad (3)$$

The effect of p is discussed in Section 5.

4.3. YolOOD Class Scores

Each candidate $c' \in \mathcal{C}_k$ contains N_c class scores which represent the model's confidence of the presence of each specific class. Since multiple cells may be responsible for the detection of an object, a cell can be assigned with multiple classes. Like in the original YOLO training procedure, we train each candidate in a multi-label fashion, *i.e.*, a candidate is not mutually exclusive. Formally, the class score for a class $n \in \{1, \dots, N_c\}$ in a specific candidate c is:

$$c_{\text{cls } n} = \begin{cases} 1 & \text{class } n \text{ is in cell} \\ 0 & \text{else} \end{cases} \quad (4)$$

4.4. Loss Function

To train YolOOD, we devise a custom loss function that is composed of two components:

- Objectness score loss -

$$\mathcal{L}_{\text{obj}} = \sum_{c' \in \mathcal{C}} \mathcal{L}_{\text{BCE}}(c'_{\text{obj}}, c_{\text{obj}}) \quad (5)$$

where \mathcal{L}_{BCE} denotes the binary cross-entropy loss.

- Class score loss -

$$\mathcal{L}_{\text{cls}} = \sum_{c' \in \mathcal{C}} \sum_{n \in \{1, \dots, N_c\}} c_{\text{obj}} \cdot \mathcal{L}_{\text{BCE}}(c'_{\text{cls } n}, c_{\text{cls } n}) \quad (6)$$

Finally, the total loss function is:

$$\mathcal{L}_{\text{total}} = \mathcal{L}_{\text{obj}} + \mathcal{L}_{\text{cls}} \quad (7)$$

4.5. YolOOD as a Multi-label Classifier

Since the core definition of a multi-label classifier's output is a single vector containing class probabilities, we aggregate YolOOD's output as follows:

$$y = \max_{n \in \{1, \dots, N_c\}} \max_{c' \in \mathcal{C}} \{\sigma(c'_{\text{obj}}) \cdot \sigma(c'_{\text{cls } n})\} \quad (8)$$

where σ denotes the sigmoid function.

4.6. YolOOD for Multi-Label OOD Detection

We propose using *YolOOD* for OOD detection in the following way:

$$\text{YolOOD}(x) = \max_{c' \in f_{\text{YolOOD}}(x)} (\sigma(c'_{\text{obj}}) * \max_{i \in \{1, \dots, N_c\}} \{\sigma(c'_{\text{cls } i})\}) \quad (9)$$

$$G(x, \tau) = \begin{cases} 1 & \text{YolOOD}(x) \geq \tau \\ 0 & \text{YolOOD}(x) < \tau \end{cases} \quad (10)$$

where τ denotes the threshold, which can be selected according to the value that yields a high fraction of in-distribution (TPR@95) data correctly classified by $G(x, \tau)$.

5. Evaluation

5.1. Experimental Setup

In-distribution datasets. We consider the following in-distribution datasets, originally proposed in [10]:

- PASCAL VOC [6] - consists of 5,717 training, 5,823 validation, and 10,991 test images across 20 class categories.
- MS-COCO [20] (2017 version) - consists of 117,266 training, 4,952 validation, and 40,670 test images across 80 class categories.

Since object detection is an extension of the multi-label problem, these datasets contain bounding box annotations, well-suited to our proposed approach. The training and validation images are used for the training process, while the test set is used as an in-distribution set for the OOD detection evaluation.

Out-of-distribution datasets. In previous studies [10, 39] proposing solutions for OOD detection in the multi-label setting, the effectiveness of the proposed method was evaluated on a subset of images from the ImageNet-22K [32] and Textures [5] datasets. However, these datasets only contain images with a single class category, resulting in an oversimplified setup.

Therefore, we propose two new benchmarks constructed from datasets which contain images associated with multiple class categories and instances, thus reflecting the complexity of the multi-label setting:

- Objects365 dataset [34] - a subset of 20 classes which do not overlap with any of the classes present in the in-distribution datasets. The specific classes in the subset are chosen according to their frequency in the dataset, *i.e.*, the 20 most common classes (*e.g.*, lamp, street lights, storage box).
- Trash Annotations in Context for Litter Detection (TACO) [27] - photos of litter taken in diverse environments. We remove overlapping class categories, which leaves us with a subset of 26 categories (*e.g.* plastic bag, carton, straw).

We consider an image as OOD if none of the classes present in it belong to the in-distribution classes. Further details about the datasets are presented in the supplementary material.

Metrics. In our evaluation, performance is measured with metrics commonly used in the OOD detection domain: (a) *FPR95* - the false positive rate of OOD samples when the true positive rate is at 95%; (b) *AuROC* - the area under the receiver operating characteristic curve; and (c) *AuPR* - the area under the precision-recall curve.

Networks architecture. We use the latest version of the YOLO object detector, YOLOv5 [14], pretrained on MS-COCO. As explained in Section 2, the network is comprised of a backbone and three detection heads. YOLOv5 provides several model sizes: nano, small, medium, *etc.*, each of which contains a different number of learnable parameters for the backbone and detection heads. We use the YOLOv5 small version, which contains $\sim 4.1M$ and $\sim 3M$ learnable parameters in the backbone and detection heads, respectively, which amounts to a total of $\sim 7.1M$ parameters. To apply our OOD detection approach, we replace the last layer of each detection head with the detection layer described in Section 4.

To perform a fair comparison between the proposed method and other state-of-the-art OOD detection methods, we train a multi-label image classifier based on *YOLOv5s*'s backbone. To this end, we replace the detection heads with three fully connected layers, resulting in a similar sized network (total of $\sim 7.1M$ parameters). This network is referred to as *YOLO-cls* in the evaluation.

Training details. For each in-distribution dataset, we fine-tune a pair of *YoLOOD* and a *YOLO-cls* models using the pretrained weights. We use the Adam optimizer [15] with an initial learning rate of 10^{-5} and 10^{-4} for the backbone and the remaining layers, respectively. The learning rate is reduced by a factor of 10 if the AuPR on the validation set does not improve for two consecutive epochs. For the *YOLO-cls* model, we apply the logistic sigmoid function on the outputs of the classification layer (*i.e.*, logits) for multi-label training.

\mathcal{D}_{out}	\mathcal{D}_{in}	PASCAL-VOC	MS-COCO
	p	FPR95 ↓ / AuROC ↑ / AuPR ↑	
Objects365 [34]	0	45.80 / 84.42 / 73.75	52.74 / 85.97 / 92.84
	0.1	38.15 / 86.98 / 75.97	44.61 / 87.94 / 93.67
	0.2	28.22 / 92.13 / 85.69	35.07 / 91.01 / 95.30
	0.3	25.79 / 93.45 / 88.72	32.19 / 91.72 / 95.64
	0.4	24.86 / 93.89 / 89.57	30.38 / 92.08 / 95.80
	0.5	24.72 / 94.05 / 89.53	29.29 / 92.58 / 96.08
	0.6	23.52 / 94.11 / 88.81	28.97 / 92.68 / 96.09
	0.7	23.80 / 93.95 / 88.45	28.69 / 92.85 / 96.21
	0.8	23.99 / 93.79 / 87.89	29.59 / 92.81 / 96.13
	0.9	24.78 / 93.48 / 87.16	29.70 / 92.76 / 96.09
	1	24.96 / 93.23 / 86.63	30.70 / 92.59 / 95.96
TACO [27]	0	49.99 / 80.48 / 88.98	40.57 / 88.49 / 98.30
	0.1	37.39 / 85.41 / 90.82	32.50 / 90.10 / 98.51
	0.2	20.93 / 93.32 / 96.16	22.30 / 93.50 / 99.10
	0.3	18.55 / 95.26 / 97.74	20.66 / 94.48 / 99.29
	0.4	16.37 / 96.02 / 98.20	18.91 / 95.09 / 99.40
	0.5	15.87 / 96.33 / 98.38	18.03 / 95.39 / 99.44
	0.6	16.44 / 96.28 / 98.38	16.42 / 95.73 / 99.49
	0.7	16.61 / 96.24 / 98.42	16.63 / 95.74 / 99.49
	0.8	19.72 / 95.53 / 98.13	16.65 / 95.82 / 99.50
	0.9	19.76 / 95.58 / 98.15	16.92 / 95.88 / 99.51
	1	19.95 / 95.55 / 98.15	19.12 / 95.60 / 99.48

Table 1. OOD detection performance on various p values (described in Section 4.2). ↓ indicates lower values are better, and ↑ indicates higher values are better.

For both of the models, the images are resized to 640×640 pixels, and applied with color-based augmentations and geometric transformations are applied to the images.

5.2. Results

Effect of responsible grid cell percentage p . We characterize the effect of the percentage p of responsible cells (described in Section 4.2). Table 1 summarizes the OOD detection performance, where p is selected from 11 evenly spaced numbers in the range $[0, 1]$. The results confirm that enlarging the number of grid cells responsible for the detection of an object substantially improves the OOD performance. Moreover, as can be seen, at some point (*e.g.*, $p = 0.7$ for MS-COCO), the benefit that a larger number of grid cells provide to OOD detection performance starts to diminish, most likely due to the non-rectangular characteristic of objects, *i.e.*, background areas are included within the bounding box. Ideally, using a dataset that contains pixel-level annotations will allow the model to learn accurate representations without irrelevant areas. The remainder of the results presented in this section are based on a *YoLOOD* model trained using the configuration $p = 0.7$, which empirically achieves the best performance.

\mathcal{D}_{out} \mathcal{D}_{in} Method	Objects365		TACO	
	PASCAL-VOC	MS-COCO	PASCAL-VOC	MS-COCO
	FPR95 ↓ / AuROC ↑ / AuPR ↑			
MaxLogit [10]	43.29 / 88.52 / 76.96	39.57 / 90.25 / 94.78	31.65 / 93.16 / 96.45	17.13 / 95.80 / 99.47
MSP [11]	60.42 / 81.92 / 69.28	62.62 / 75.52 / 86.24	55.66 / 85.97 / 93.18	38.48 / 86.43 / 98.02
ODIN [18]	43.29 / 88.52 / 76.96	39.57 / 90.25 / 94.78	31.65 / 93.16 / 96.45	17.13 / 95.80 / 99.47
Mahalanobis [17]	70.53 / 76.52 / 65.07	88.02 / 55.75 / 71.66	31.10 / 91.60 / 95.64	60.69 / 78.68 / 96.01
JointEnergy [39]	43.41 / 89.17 / 81.38	40.61 / 91.89 / 96.31	28.80 / 93.95 / 97.20	14.50 / 96.52 / 99.56
YoOOD	23.80 / 93.95 / 88.45	28.69 / 92.85 / 96.21	16.61 / 96.24 / 98.42	16.63 / 95.74 / 99.49

Table 2. Comparison of the OOD detection performance of YoOOD vs. state-of-the-art methods. ↓ indicates lower values are better, and ↑ indicates higher values are better. Bold indicates superior results.

YoOOD vs. state-of-the-art OOD detection methods.

We compare our approach to state-of-the-art OOD detection methods: (a) MaxLogit [10], (b) Maximum Softmax Probability (MSP) [11], (c) ODIN [18], (d) Mahalanobis [17], and (e) JointEnergy [39]. Among the different OOD detection methods, YoOOD outperforms all baselines and state-of-the-art approaches, including the multi-label OOD detection method, *JointEnergy*. Specifically, when the networks are trained on the PASCAL-VOC and MS-COCO datasets and the OOD detection is evaluated on the subset of the Object365 OOD dataset, *YoOOD* reduces the FPR95 by 19.49% and 10.88%, respectively, compared to the best performing method.

It should also be noted that in comparison to the other methods examined, the Mahalanobis method shows poor performance. In [39], the authors hypothesize that the Mahalanobis method may not be well suited for the multi-label task, since it is based on the assumption that feature representation forms class-conditional Gaussian distributions. This assumption also holds in our case, however from a different perspective, in which the *YOLO-cls* backbone used for the evaluation was originally trained for the object detection task, learning different feature representations.

Objectness score vs. class score vs. joint objectness and class scores. We also perform an analysis to examine the effect of different aggregation methods on the candidates' output scores, *i.e.*, objectness and class scores. We consider two different approaches in addition to the regular YoOOD described in Equation 9 (which uses a joint probability between the objectness and class scores):

$$\text{YoOOD}_{\text{Cls}}(x) = \max_{c' \in f_{\text{YoOOD}}(x)} \left(\max_{n \in \{1, \dots, N_c\}} \{\sigma(c'_{\text{cls } n})\} \right) \quad (11)$$

$$\text{YoOOD}_{\text{Obj}}(x) = \max_{c' \in f_{\text{YoOOD}}(x)} (\sigma(c'_{\text{obj}})) \quad (12)$$

In Figure 4, we can see that when using the objectness and class scores separately ($\text{YoOOD}_{\text{Obj}}$ and $\text{YoOOD}_{\text{Cls}}$, respectively), the objectness contributes the most to distinguishing between in-distribution and OOD samples. However, when using a joint probability, the results improve.

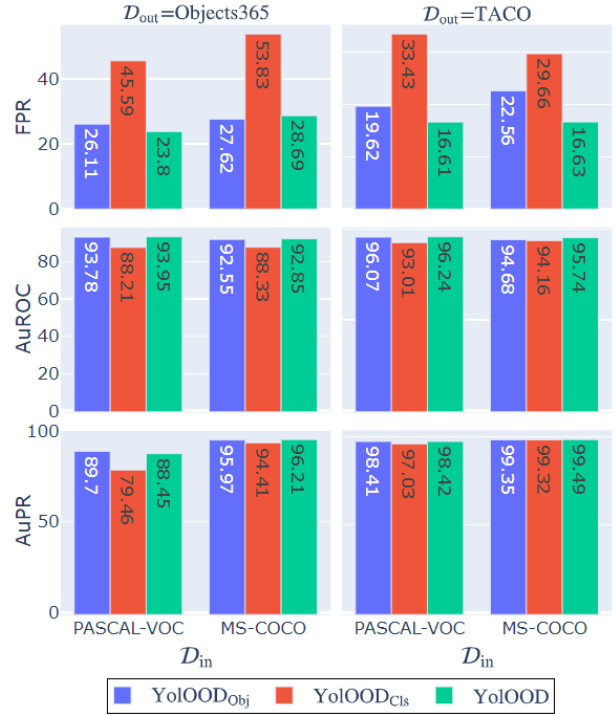


Figure 4. Comparison of OOD detection performance using different aggregation methods on YoOOD candidates' output scores (described in Section 5.2).

Combining YoOOD with JointEnergy. Wang *et al.* [39] presented the JointEnergy technique in the following way:

$$E_{y_n}(x) = -\log(1 + e^{f_{y_n}(x)})$$

$$E_{\text{joint}}(x) = \sum_{n=1}^{N_c} -E_{y_n}(x) \quad (13)$$

where $f_{y_n}(x)$ denotes the logit of the n^{th} class.

Since YoOOD's output can be transformed into a single vector of class probabilities (as shown in Section 4.5), JointEnergy can be applied and used with the YoOOD architecture. Therefore, instead of applying the sigmoid function on

\mathcal{D}_{out}	\mathcal{D}_{in} Model	PASCAL-VOC	MS-COCO
		FPR95 ↓ / AuROC ↑ / AuPR ↑	FPR95 ↓ / AuROC ↑ / AuPR ↑
Objects365	YOLO-cls	43.41 / 89.17 / 81.38	40.61 / 91.89 / 96.31
	YoOOD	25.38 / 94.11 / 90.59	29.22 / 93.83 / 97.17
TACO	YOLO-cls	28.80 / 93.95 / 97.20	14.50 / 96.52 / 99.56
	YoOOD	16.84 / 96.52 / 98.61	14.57 / 96.38 / 99.58

Table 3. OOD detection performance comparison when applying JointEnergy on YoOOD and YOLO-cls networks.

the objectness and class scores as shown in Equation 9, we apply the energy function E_{y_n} . The use of YoOOD combined with JointEnergy can be described in the following way:

$$\begin{aligned} \text{YoOOD}_{\text{Energy}}(x) = & \max_{n \in \{1, \dots, N_c\}} \max_{c' \in \mathcal{C}_{\text{YoOOD}}(x)} \{-E_{y_i}(c'_{\text{obj}}) \cdot -E_{y_n}(c'_{\text{cls } n})\} \\ \text{YoOOD}_{\text{JointEnergy}}(x) = & \sum \text{YoOOD}_{\text{Energy}} \quad (14) \end{aligned}$$

$\text{YoOOD}_{\text{Energy}}$ applies the energy function E_{y_n} to all of its outputs (both objectness and class scores) to extract the highest score for each class $n \in \{1, \dots, N_c\}$ from the candidate set \mathcal{C} . Finally, as suggested in [39], $\text{YoOOD}_{\text{JointEnergy}}$ combines label-wise energies over all labels for a single OOD score.

Table 3 presents the results obtained when JointEnergy is used in conjunction with YoOOD, as well as with a regular image classifier (YOLO-cls). As can be seen, YoOOD’s OOD detection performance improves when JointEnergy is applied compared to the YOLO-cls network. Moreover, in most cases, $\text{YoOOD}_{\text{JointEnergy}}$ demonstrates improved performance on the AuROC and AuPR metrics compared to the regular YoOOD.

Effectiveness of different aggregation functions. Since YoOOD’s output is comprised of three detection heads, we consider using different aggregation functions between them, *i.e.* instead of combining all of the candidates into one large set $\mathcal{C} = \bigcup_k \mathcal{C}_k$, we extract the best candidate from each set \mathcal{C}_k and only then apply the aggregation function. More formally, we replace Equation 9 with the following:

$$\text{agg} \max_{k \in \{1, 2, 3\}} (c_{\text{obj } k} * \max_{n \in \{1, \dots, N_c\}} \{c_{\text{cls } n}\}) \quad (15)$$

where agg can either be the summation or multiplication functions. In addition, we also examine the effect of different aggregation functions on the class score output vector (similar to [39] which proposes summing energies over all of the labels).

In general, the results presented in Table 4 show that using different aggregation functions both for the detection heads and the output vectors does not improve the OOD detection performance. Furthermore, as opposed to [39], summing over the output scores does not benefit the OOD

Output Agg.	\mathcal{D}_{in} Head Agg.	PASCAL-VOC	MS-COCO
		FPR95 ↓ / AuROC ↑ / AuPR ↑	FPR95 ↓ / AuROC ↑ / AuPR ↑
Max	Sum	24.03 / 93.94 / 88.01	29.83 / 92.41 / 95.96
	Multiply	24.23 / 93.93 / 87.92	30.01 / 92.39 / 95.97
	Max	23.80 / 93.95 / 88.45	28.69 / 92.85 / 96.21
	Sum	48.38 / 77.92 / 63.93	70.23 / 71.42 / 84.67
Sum	Multiply	24.61 / 91.64 / 84.64	30.92 / 90.08 / 95.04
	Max	25.38 / 94.11 / 90.59	29.26 / 93.86 / 97.17

Table 4. OOD detection performance when using different combinations of aggregation functions for YoOOD’s detection heads and class scores output vector. The subset from Object365 dataset serves as the OOD dataset.

detection performance in our case, and when used in conjunction with summing over the scores of the detection heads, the performance deteriorates.

6. Discussion

Limitations. Usually, models deployed in the real-world are trained on a proprietary dataset that requires manual labeling by a human. Labeling a classification dataset involves a simple GUI program that allows the annotator to choose the specific classes for a given image. However, a limitation of our method is that it requires ground-truth bounding boxes, which is a more complex and expensive procedure, compared to labeling standard image classification datasets. To bridge the gap between the standard labeling procedure and our method’s requirement of ground-truth bounding boxes, we propose using an automatic procedure that extracts bounding boxes from a given dataset – self-supervised object discovery models [33, 35, 38, 40] which are able to detect objects in an image without being trained on specific classes. This technique extracts all of the bounding boxes from the image (without classifying the class categories), which can then be followed by a standard classification labeling procedure.

7. Conclusion

In this paper, we presented YoOOD – an OOD detection approach for the underexplored multi-label classification domain which utilizes the main concepts of object detectors, and more specifically, the YOLO object detector. We demonstrated how all parts of an input image can be exploited to model both in-distribution and OOD data. In our evaluation, we performed a comprehensive set of experiments on various benchmark datasets and presented two new OOD benchmark datasets that better reflect the complexity of the multi-label domain. Our approach achieved state-of-the-art performance compared to the baselines and state-of-the-art OOD detection methods examined.

References

- [1] Guy Amit, Moshe Levy, Ishai Rosenberg, Asaf Shabtai, and Yuval Elovici. Food: Fast out-of-distribution detector. In *2021 International Joint Conference on Neural Networks (IJCNN)*, pages 1–8. IEEE, 2021. 1
- [2] Alexey Bochkovskiy, Chien-Yao Wang, and Hong-Yuan Mark Liao. Yolov4: Optimal speed and accuracy of object detection. *arXiv preprint arXiv:2004.10934*, 2020. 1, 2, 3
- [3] Kai Chen, Jiangmiao Pang, Jiaqi Wang, Yu Xiong, Xiao-xiao Li, Shuyang Sun, Wansen Feng, Ziwei Liu, Jianping Shi, Wanli Ouyang, et al. Hybrid task cascade for instance segmentation. In *Proceedings of the IEEE conference on computer vision and pattern recognition*, pages 4974–4983, 2019. 1
- [4] Liang-Chieh Chen, George Papandreou, Iasonas Kokkinos, Kevin Murphy, and Alan L Yuille. Semantic image segmentation with deep convolutional nets and fully connected crfs. *arXiv preprint arXiv:1412.7062*, 2014. 1
- [5] Mircea Cimpoi, Subhansu Maji, Iasonas Kokkinos, Sammy Mohamed, and Andrea Vedaldi. Describing textures in the wild. In *Proceedings of the IEEE conference on computer vision and pattern recognition*, pages 3606–3613, 2014. 5
- [6] Mark Everingham, SM Eslami, Luc Van Gool, Christopher KI Williams, John Winn, and Andrew Zisserman. The pascal visual object classes challenge: A retrospective. *International journal of computer vision*, 111(1):98–136, 2015. 5
- [7] Golnaz Ghiasi, Tsung-Yi Lin, and Quoc V Le. Nas-fpn: Learning scalable feature pyramid architecture for object detection. In *Proceedings of the IEEE/CVF conference on computer vision and pattern recognition*, pages 7036–7045, 2019. 2
- [8] Kaiming He, Georgia Gkioxari, Piotr Dollár, and Ross Girshick. Mask r-cnn. In *Proceedings of the IEEE international conference on computer vision*, pages 2961–2969, 2017. 2
- [9] Kaiming He, Xiangyu Zhang, Shaoqing Ren, and Jian Sun. Delving deep into rectifiers: Surpassing human-level performance on imagenet classification. In *Proceedings of the IEEE international conference on computer vision*, pages 1026–1034, 2015. 1
- [10] Dan Hendrycks, Steven Basart, Mantas Mazeika, Mohammadreza Mostajabi, Jacob Steinhardt, and Dawn Song. Scaling out-of-distribution detection for real-world settings. *arXiv preprint arXiv:1911.11132*, 2019. 2, 5, 7
- [11] Dan Hendrycks and Kevin Gimpel. A baseline for detecting misclassified and out-of-distribution examples in neural networks. *arXiv preprint arXiv:1610.02136*, 2016. 2, 7
- [12] Dan Hendrycks, Mantas Mazeika, and Thomas Dietterich. Deep anomaly detection with outlier exposure. *arXiv preprint arXiv:1812.04606*, 2018. 2
- [13] Rui Huang, Andrew Geng, and Yixuan Li. On the importance of gradients for detecting distributional shifts in the wild. *Advances in Neural Information Processing Systems*, 34:677–689, 2021. 1, 2
- [14] Glenn Jocher. ultralytics/yolov5: v6.0 - yolov5n 'nano' models, roboflow integration, tensorflow export, opencv dnn support, oct 2021. 1, 2, 3, 4, 6
- [15] Diederik P Kingma and Jimmy Ba. Adam: A method for stochastic optimization. *arXiv preprint arXiv:1412.6980*, 2014. 6
- [16] Alex Krizhevsky, Ilya Sutskever, and Geoffrey E Hinton. Imagenet classification with deep convolutional neural networks. In *Advances in neural information processing systems*, pages 1097–1105, 2012. 1
- [17] Kimin Lee, Kibok Lee, Honglak Lee, and Jinwoo Shin. A simple unified framework for detecting out-of-distribution samples and adversarial attacks. *Advances in neural information processing systems*, 31, 2018. 1, 2, 7
- [18] Shiyu Liang, Yixuan Li, and Rayadurgam Srikant. Enhancing the reliability of out-of-distribution image detection in neural networks. *arXiv preprint arXiv:1706.02690*, 2017. 1, 2, 7
- [19] Tsung-Yi Lin, Piotr Dollár, Ross Girshick, Kaiming He, Bharath Hariharan, and Serge Belongie. Feature pyramid networks for object detection. In *Proceedings of the IEEE conference on computer vision and pattern recognition*, pages 2117–2125, 2017. 2, 3
- [20] Tsung-Yi Lin, Michael Maire, Serge Belongie, James Hays, Pietro Perona, Deva Ramanan, Piotr Dollár, and C Lawrence Zitnick. Microsoft coco: Common objects in context. In *European conference on computer vision*, pages 740–755. Springer, 2014. 2, 5
- [21] Shu Liu, Lu Qi, Haifang Qin, Jianping Shi, and Jiaya Jia. Path aggregation network for instance segmentation. In *Proceedings of the IEEE conference on computer vision and pattern recognition*, pages 8759–8768, 2018. 2
- [22] Wei Liu, Dragomir Anguelov, Dumitru Erhan, Christian Szegedy, Scott Reed, Cheng-Yang Fu, and Alexander C Berg. Ssd: Single shot multibox detector. In *European conference on computer vision*, pages 21–37. Springer, 2016. 1, 2
- [23] Weitang Liu, Xiaoyun Wang, John Owens, and Yixuan Li. Energy-based out-of-distribution detection. *Advances in Neural Information Processing Systems*, 33:21464–21475, 2020. 2
- [24] David Macêdo, Tsang Ing Ren, Cleber Zanchettin, Adriano LI Oliveira, and Teresa Ludermir. Entropic out-of-distribution detection. In *2021 International Joint Conference on Neural Networks (IJCNN)*, pages 1–8. IEEE, 2021. 1, 2
- [25] Sina Mohseni, Mandar Pitale, JBS Yadawa, and Zhangyang Wang. Self-supervised learning for generalizable out-of-distribution detection. In *Proceedings of the AAAI Conference on Artificial Intelligence*, volume 34, pages 5216–5223, 2020. 2
- [26] Anh Nguyen, Jason Yosinski, and Jeff Clune. Deep neural networks are easily fooled: High confidence predictions for unrecognizable images. In *Proceedings of the IEEE conference on computer vision and pattern recognition*, pages 427–436, 2015. 1, 2
- [27] Pedro F Proença and Pedro Simões. Taco: Trash annotations in context for litter detection. *arXiv preprint arXiv:2003.06975*, 2020. 2, 6

- [28] Joseph Redmon, Santosh Divvala, Ross Girshick, and Ali Farhadi. You only look once: Unified, real-time object detection. In *Proceedings of the IEEE conference on computer vision and pattern recognition*, pages 779–788, 2016. 1, 3
- [29] Joseph Redmon and Ali Farhadi. Yolo9000: better, faster, stronger. In *Proceedings of the IEEE conference on computer vision and pattern recognition*, pages 7263–7271, 2017. 3
- [30] Joseph Redmon and Ali Farhadi. Yolo3: An incremental improvement. *arXiv preprint arXiv:1804.02767*, 2018. 1, 2, 3
- [31] Shaoqing Ren, Kaiming He, Ross Girshick, and Jian Sun. Faster r-cnn: Towards real-time object detection with region proposal networks. *Advances in neural information processing systems*, 28, 2015. 1, 2
- [32] Olga Russakovsky, Jia Deng, Hao Su, Jonathan Krause, Sanjeev Satheesh, Sean Ma, Zhiheng Huang, Andrej Karpathy, Aditya Khosla, Michael Bernstein, Alexander C. Berg, and Li Fei-Fei. ImageNet Large Scale Visual Recognition Challenge. *International Journal of Computer Vision (IJCV)*, 115(3):211–252, 2015. 2, 5
- [33] Kuniaki Saito, Ping Hu, Trevor Darrell, and Kate Saenko. Learning to detect every thing in an open world. In *European Conference on Computer Vision*, pages 268–284. Springer, 2022. 8
- [34] Shuai Shao, Zeming Li, Tianyuan Zhang, Chao Peng, Gang Yu, Xiangyu Zhang, Jing Li, and Jian Sun. Objects365: A large-scale, high-quality dataset for object detection. In *Proceedings of the IEEE/CVF international conference on computer vision*, pages 8430–8439, 2019. 2, 6
- [35] Oriane Siméoni, Gilles Puy, Huy V Vo, Simon Roburin, Spyros Gidaris, Andrei Bursuc, Patrick Pérez, Renaud Marlet, and Jean Ponce. Localizing objects with self-supervised transformers and no labels. In *BMVC-British Machine Vision Conference*, 2021. 8
- [36] Yiyao Sun, Chuan Guo, and Yixuan Li. React: Out-of-distribution detection with rectified activations. *Advances in Neural Information Processing Systems*, 34:144–157, 2021. 1, 2
- [37] Mingxing Tan, Ruoming Pang, and Quoc V Le. Efficientdet: Scalable and efficient object detection. In *Proceedings of the IEEE/CVF conference on computer vision and pattern recognition*, pages 10781–10790, 2020. 2
- [38] Huy V. Vo, Elena Sizikova, Cordelia Schmid, Patrick Pérez, and Jean Ponce. Large-scale unsupervised object discovery. In *Advances in Neural Information Processing Systems 35 (NeurIPS)*, 2021. 8
- [39] Haoran Wang, Weitang Liu, Alex Bocchieri, and Yixuan Li. Can multi-label classification networks know what they don’t know? *Advances in Neural Information Processing Systems*, 34:29074–29087, 2021. 1, 2, 5, 7, 8
- [40] Yangtao Wang, Xi Shen, Shell Xu Hu, Yuan Yuan, James L Crowley, and Dominique Vaufreydaz. Self-supervised transformers for unsupervised object discovery using normalized cut. In *Proceedings of the IEEE/CVF Conference on Computer Vision and Pattern Recognition*, pages 14543–14553, 2022. 8